OPEN ACCESS
IOP Publishing
Nanotechnology

Nanotechnology **26** (2015) 155101 (9pp)
doi:10.1088/0957-4484/26/15/155101

Statistical prediction of nanoparticle delivery: from culture media to cell

M Rowan Brown[1], Nicole Hondow[2], Rik Brydson[2], Paul Rees[1], Andrew P Brown[2] and Huw D Summers[1]

[1] College of Engineering, Swansea University, Swansea, SA2 8PP, UK
[2] Institute for Materials Research, University of Leeds, Leeds, LS2 9JT, UK

E-mail: m.r.brown@swansea.ac.uk

Received 12 December 2014, revised 12 February 2015
Accepted for publication 14 February 2015
Published 23 March 2015

Abstract

The application of nanoparticles (NPs) within medicine is of great interest; their innate physicochemical characteristics provide the potential to enhance current technology, diagnostics and therapeutics. Recently a number of NP-based diagnostic and therapeutic agents have been developed for treatment of various diseases, where judicious surface functionalization is exploited to increase efficacy of administered therapeutic dose. However, quantification of heterogeneity associated with absolute dose of a nanotherapeutic (NP number), how this is trafficked across biological barriers has proven difficult to achieve. The main issue being the quantitative assessment of NP number at the spatial scale of the individual NP, data which is essential for the continued growth and development of the next generation of nanotherapeutics. Recent advances in sample preparation and the imaging fidelity of transmission electron microscopy (TEM) platforms provide information at the required spatial scale, where individual NPs can be individually identified. High spatial resolution however reduces the sample frequency and as a result dynamic biological features or processes become opaque. However, the combination of TEM data with appropriate probabilistic models provide a means to extract biophysical information that imaging alone cannot. Previously, we demonstrated that limited cell sampling via TEM can be statistically coupled to large population flow cytometry measurements to quantify exact NP dose. Here we extended this concept to link TEM measurements of NP agglomerates in cell culture media to that encapsulated within vesicles in human osteosarcoma cells. By construction and validation of a data-driven transfer function, we are able to investigate the dynamic properties of NP agglomeration through endocytosis. In particular, we statistically predict how NP agglomerates may traverse a biological barrier, detailing inter-agglomerate merging events providing the basis for predictive modelling of nanopharmacology.

Keywords: nanoparticle, nonhomogeneous Poisson process, transmission electron microscopy, nanotherapeutic

(Some figures may appear in colour only in the online journal)

Introduction

The application of nanoparticles (NPs) within medicine is of great interest; their innate physicochemical characteristics provide the potential to enhance current technology, diagnostics and therapeutics. In recent years a number of NP-based diagnostic and therapeutic agents have been developed for treatment of various cancers, where surface functionality has been exploited to provide more effective routes to administration of therapeutic dose [1, 2]. As delivery systems NPs provide an improved means to detect abnormalities at the molecular scale; surface functionality providing increased targeting efficiency and controlled release of therapeutic dose

over a user-defined period; a thorough review is provided by Zhang *et al* [3]. Additionally, NPs have improved the sensitivity and specificity of many imaging platforms. In particular, superparamagnetic NPs now play a key role in magnetic resonance imaging, providing enhanced image contrast and increased resolution to inform and quantify many tissue abnormalities (see Na *et al* [4] for examples).

Despite success in these areas, application of NP technology or quantification of NP dose at the individual cellular-level is still at an infant stage. Specifically, detailing the influence that the myriad of biophysical processes have on NP agglomeration, transport within biological media, cellular uptake, internalization and redistribution has proven difficult to quantify. This shortcoming is directly related to the inability of high-throughput time-lapse systems to provide rigorous cytometric measurement and analyses of the evolution path of NPs on an appropriate spatial scale (i.e. the individual NP (nm)). If NP-based medicine is to be truly realized in future years it is an absolute that the community are able to accurately (i) quantify the internalized nanomaterial dose as opposed to that simply applied [5, 6], (ii) determine the biological consequences associated with this actual dose and (iii) predict how the dose evolves over time.

Electron microscopy, in particular transmission electron microscopy (TEM), is a technical platform that can deliver information at the required spatial scale, where individual NPs can be identified, in terms of both number and spatial location [7]. Recent *in vitro* studies have detailed the impact of gold NP agglomeration on several cell lines [8, 9], where this is important because comparisons of NP agglomerate size measured in water and cell culture media report increases in size for the latter [10]. We have previously demonstrated a method in which NP dispersion can be rapidly frozen and imaged in the TEM, with representative agglomerate dimensions measured [11]. This provides more precise imaging of actual NP agglomerate state in which a NP agglomerate size and distribution is more accurately determined, a fundamental criterion for the continued development of a nanomedicine. TEM has also been applied to study the cellular uptake of NPs to human mammary cells by endocytosis, with outputs suggesting initial sequestration in early endosomes followed by translocation to late endosomes or lysosomes [12]. In addition, Krpetic *et al* have previously used TEM to track the intracellular distribution of peptide modified gold NPs at several time points, covering initial membrane bound encapsulation and release, and through to clearing of the particles from the analyzed cells [13].

Application of this technology however comes with an intrinsic compromise that limits temporal sampling when compared to flow cytometry and current optical microscopy platforms. Due to reduced temporal sampling many electron microscopy contributions to research in nanomedicine are purely qualitative, however, there is a growing research community that are developing novel methodologies that provide quantitative biophysical insight of contiguous TEM measurements [14–16]. Specifically, utilizing TEM in conjunction with appropriate stochastic or statistical methods that provide a bridge between measurement points can be exploited to provide unresolvable information of the underlying biophysical processes in this interval.

In this work, we apply the concept of statistical analysis to link distinct spatiotemporal TEM measurements [15] to investigate the transport of NP agglomerates in cell culture media, to that within endosome compartments in human osteosarcoma cells (U2-OS cell-line). The NPs employed are QTracker 705 nm CdTe/ZnS quantum dots at a 10 nM dose; we have significant experience incorporating these NPs within U2-OS cellular systems and have demonstrated that they are toxicologically and pharmacodynamically inert at this dosage [17, 18], and that they may be utilized to extract meaningful biological parameters, see [15, 17, 19–24] for examples. QTracker 705 nm quantum dots are specifically targeted for endocytic uptake; the NPs have an organic coating, composed of arginine-rich targeting peptides conjugated to biotin bonded to streptavidin and the arginine-rich peptides can lead to cellular uptake via micropinocytosis [25].

We image and characterize 500 distinct NP agglomerates/aggregates in culture media and within endosome compartment cells respectively, the latter following the 1 h exposure to the NP rich culture media. For clarity, we refer to NP clusters in culture media as agglomerates and those within endosomes as aggregates. Each of the NP agglomerates/aggregates imaged via TEM is randomly selected, in the latter case we first randomly select 100 distinct cells from a cellular population comprising of $>10^4$ cells and subsequently select stochastically 500 endosomes from within this cellular subpopulation. In both spatiotemporal cases the number of individual NPs per agglomerate/aggregate is determined [11]. Previously, we have shown stochastic sampling of high-resolution low frequency TEM images in this manner is capable of capturing cellular heterogeneity in NP uptake and further redistribution within daughter cells through mitosis. Specifically, we demonstrated that stochastic sampling of probability mass functions (PMFs) that encapsulate NP number per endosome and NP aggregate number per cell can be utilized to provide the total quantum dot fluorescent intensity per cell for 10^4 in-silico cells. It was established that the in-silico population accurately recreated and predicted corresponding high-throughput flow cytometry measurements [15].

Analyzing the collected TEM images we construct the PMFs that encapsulate system heterogeneity associated with NP agglomerates/aggregates size (i.e. number of constituent NPs) in culture media and in endosome compartments following 1 h NP exposure.

We demonstrate that transition of states between the two PMFs can be achieved by considering the combined biophysical processes of NP transport [26] and cellular uptake as a nonhomogeneous Poisson process (NHPP), where the rate parameter that describes NP agglomerate aggregation at the cellular surface or during endocytosis is driven by actual TEM measurements. Statistical sampling of the NHPP returns the number of NP agglomerates from within the culture media that have attached to an active endocytic domain on the cell surface and have subsequently been encapsulated within an

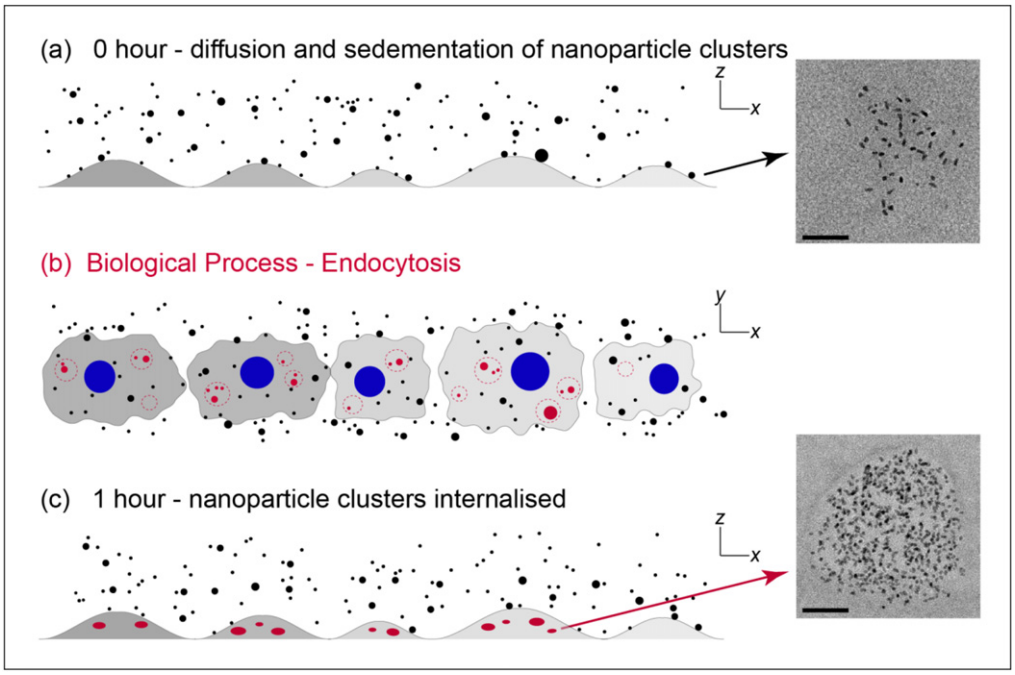

Figure 1. Schematic illustrating the processes of nanoparticle sedimentation and cellular uptake over a 1 h period. (a) 0 h—NP agglomerate are introduced to the cell media; (previously measured NP agglomerate variability is represented by black disks of varying diameter, an example of a bright field TEM image of a NP agglomerate in media is shown on the RHS—scale bar 75 nm) [11]. (b) Biological process—we observe the random uptake [24] of NP agglomerates into discrete cellular vesicles, dashed red circles illustrate an endoctyic active region on the surface of the cell that are undergoing internalization. (c) 1 h post nanoparticle load; previously distinct NP agglomerates are internalized as aggregates through an endocytic pathway, the agglomerates are now merged into single discrete aggregate within the endosome (red circles, an example of a TEM image of a NP agglomerate within a cellular endosome is shown on the RHS—scale bar 100 nm).

endosome through one of the many endocytic pathways. The PMF of the number of NPs per in-silico endosome is then deduced and compared with the correspond PMF actually measured via TEM; through difference minimization we are able to recover the average lifetime of an active endocytic event and the mean area of the domain and show these are commensurate with direct measurements of clathrin-coated pits through high-resolution optical microscopy techniques [27, 28], validating the applicability of the methodology. This data-driven methodology provides a means to intrinsically embed internalized nanomaterial dose within the in-silico endosome population [5, 6] and statistically establish how the cell media NP dose has translated across the biological membrane into endosome compartments in so doing addressing important unmet requirements of associated with quantification of nanotheraputics.

Materials and methods

TEM

TEM was conducted on an FEI Tecnai F20 FEG-TEM operated at 200 kV and equipped with a Gatan Orius SC600A CCD camera. Commercially available targeted nanocrystals, QTracker705 quantum dots dispersed at 10 nM in McCoys 5A cell culture media containing 10% fetal calf serum were examined using the plunge-freeze method previously reported [11]. Briefly, this involves rapidly freezing a blotted 3.5 μL droplet of the suspension on a glow discharge treated carbon support film in to liquid ethane. Following this, the sample was warmed to room temperature using a rotary pumped vacuum desiccator. In cell uptake experiments, U2OS cells maintained in McCoys 5a media and 10% fetal calf serum at 37 °C in an atmosphere of 5% CO_2 were loaded with the commercially available targeted nanocrystals, QTracker705 at a 10 nM concentration [15, 17]. Samples were prepared for TEM in a standard manner [11, 15] with no additional heavy metal stain added to the resulting 100 nm thick sections.

NP agglomerate—translation from cell culture media to endosome compartment

In the following we present an overview of NP particle traverse from media to endosome compartment. We describe qualitatively the key biophysical states (i) NPs are loaded into culture media (outside the cell) at the start of the experiment, (ii) during the experiment, NPs are transported through the media to the cell surface and may be internalized through an active endocytic pathway and (iii) 1 h post NP load, the cellular population are biologically fixed and no further NP particle internalization by the cells takes place. Time points (i) and (iii) coincide with previously reported TEM measurements of NP agglomerates in media [11] and in cellular vesicles [15]; 500 agglomerates were imaged at random and the number of individual NPs per agglomerate, x, was deduced via a bespoke image analysis routine [11]. The data

measured at these distinct time points are embedded within our model, intrinsically incorporating system heterogeneity.

Figure 1(a) is a schematic of the experimental set-up at the beginning of the experiment (0–h) and illustrates a cellular population (grey protuberances) in media subject to a NP dose of 10 nM [11, 15]. Hondow *et al* [11] previously reported that QTracker 705 NPs agglomerate indiscriminately in culture media, (see results) the high heterogeneity of x is illustrated here by the variance associated with the radii of the black disks. A TEM image of a NP agglomerate captured in media [11] is shown on the right-hand side of the figure (scale bar is 75 nm). During the 1 h interval of the experiment NP agglomerates are transported to the cell surface via diffusion and sedimentation processes. The mean transport rates of the differently sized NP agglomerates, $\gamma(x)$, can be accurately determined through application of the *in vitro* sedimentation, diffusion and dosimetry (ISDD) model [26] specific to the NP and experimental set-up considered.

At the cell surface NP agglomerates can be captured by one of the many endocytic pathways and subsequently be internalized by the cell into discrete endosome compartments [29]. A simplified view of this complex biophysical process is shown in figure 1(b). The figure displays a plan view of the cellular population; cells are represented by the grey domains, blue circles are corresponding cell nuclei and the red-dashed circles represent areas on the cell surface where an endocytic event is taking place. We define such to areas to be endosome active domains (EADs). The red and black disks in the figure represent NP agglomerates inside or outside these domains respectively. For simplicity, we assume (i) that NP agglomerate attachment to receptors within individual EAD are irreversible and all attached agglomerates are subsequently aggregated and internalized by the cell (red) and (ii) over the duration of the experiment EADs appear randomly (spatio-temporally) on the cell surface and persist for a mean lifetime, τ, where $\tau \ll 1$ h [27]. The latter criterion together with the approximation that NP agglomerate transport to the cell is deduced via a mean rate over the duration of the entire experiment, suggests that the number of distinct NP agglomerates that impinge on a given EAD, $N(x)$, is intrinsically variable. We postulate that the variability of $N(x)$ is well described if we consider the combined biophysical processes of NP agglomerate transport and EAD attachment as an arrival event within a NHPP. The number of random arrivals of agglomerate with x constituent NPs is then given by:

$$N(x) = \frac{\lambda(x)^x e^{\lambda(x)}}{x!}, \tag{1}$$

where the magnitude of rate parameter $\lambda(x)$ comprises two principle components:

$$\lambda(x) = \alpha(x)E(x). \tag{2}$$

The first component $\alpha(x)$ is driven by the experimental system under investigation and is further split into the following expression:

$$\alpha(x) = N_{\mathrm{EAD}}\,\gamma(x)\tau, \tag{3}$$

where N_{EAD} is the mean number of NPs that settle on a EAD over the period τ (see below for calculation of N_{EAD}). As outlined above $\gamma(x)$ is the deterministic rate at which a NP agglomerate is transported to the surface of the cell during the course of the experiment (see ISDD model below). The mean lifetime or turnover rate an endocytic event τ, is the implicit fitting parameter of this methodology; the consequences of τ variability is addressed and discussed in the results section of the manuscript. The second component $E(x)$ is a numerical weighting coefficient, it is the product of the PMF associated with the number of individual NPs per agglomerate measured in media ($P^M(x)$, see results) and the experimentally determined range of x itself:

$$E(x) = P^M(x).x. \tag{4}$$

This parameter is paramount in our data-driven methodology, its magnitude is prescribed by previously measured data, which both limits and biases the values of $N(x)$ accordingly via application of equation (1) (random sampling of the NHPP). Together equations (1)–(4) provide a data-driven and biophysically viable methodology to estimate the number of NP agglomerates per EAD, $N(x)$, over the course of its lifetime τ. Finally, figure 1(c) is a schematic of the experimental set-up at the end of the experiment (1 h); the diagram indicates that previously distinct NP agglomerates within an individual EAD have been condensed into a single aggregate through the internalization process (red ellipses); where total NP number is conserved. A TEM image of a NP aggregate within an endosome is shown on the right-hand side of the figure (scale bar is 100 nm). The total number of NPs per endosome is simply deduced via the summation:

$$N_E = \sum_x N(x)x. \tag{5}$$

Using equation (5) we can stochastically generate corresponding data to that measured experimentally. Specifically, we can calculate N_E for 500 simulated endosomes and determine their corresponding probability mass distribution to compare with that deduced experimentally within endosome compartments 1 h post NP load.

In vitro ISDD model

The ISDD model was used to calculate the transport rates of QTracker 705 CdTe/ZnS quantum dot agglomerates in the cell culture media in [11]. A comprehensive review of the equations governing particle diffusion and sedimentation are provided by Hinderliter *et al* [26], furthermore the paper provides a MATLAB script to solve the various equations and numerous applications of the model. We modified the ISDD model parameters to make the solution specific for QTracker 705 (CdTe) quantum dots and the biological assay used; all parameters used are displayed in table 1.

The ISDD model provides an estimation of the diffusion and sedimentation rates as a function of number of NPs per agglomerate for a media depth of 287 μm over the 1 h period of the experiment; these are displayed in figure 2, blue line with 'x' markers and green line with circle markers

Table 1. Empirical values of experimental and ISDD parameters.

NP	CdTe
NP Concentration (nMol), N_c	10
Major Axis Length (nm)[a]	10
Packing fraction (nm^{-2})[a]	0.02
Fractal dimension[b]	2.3
Area of flask, A_f (m^2)	75×10^{-4}
Media volume (mL), V^M	2
Media depth (μm)	287

[a] Hondow *et al* [11].
[b] Estimated as $d_f + 1$ (see Falconer [31], chapter 6), where d_f is the fractal dimension of the 2d projection of the actual 3d NP aggregate, i.e. TEM image.

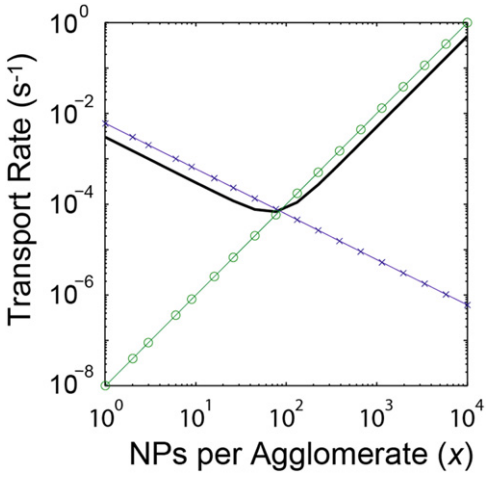

Figure 2. Simulated transport properties of CdTe NP agglomerate generated by the ISDD model. The solid black line is the mean transport rate of agglomerate to the cell surface, $\gamma(x)$. The curves associated with the blue 'x' and green circle markers indicate the individual diffusion and sedimentation rates respectively. The dominant transport mechanism switches from diffusion to sedimentation for $x > 100$ NPs. The minimum of $\gamma(x)$ at $x \sim 100$ NPs suggests agglomerates around this size are transported least rapidly to the cell surface.

respectively. The solid black curve in figure 3 is the mean agglomerate transport rate as a function of the number of NPs per agglomerate, $\gamma(x)$, which is an average of these two processes and is employed within equation (3) to estimate the number of NPs per agglomerate dependent, Poisson distributed, integer multiplier in equations (1) and (5). The ISDD calculation predicts that $\gamma(x)$ is a minimum for $x \sim 100$ NPs per agglomerate; that is agglomerates of this size are the slowest to reach the cell surface; above and below this value transport is dominated by sedimentation and diffusion respectively.

Calculation of the mean number of NPs per endocytic active domain N_{EAD}

From the experimental parameters given in table 1 we can estimate N_{AER} from the following expression:

$$N_{EAD} = N_f \times \frac{A_{EAD}}{A_f}, \tag{6}$$

here N_f is the number of NPs in the culture flask, A_f is the area of the culture flask and A_{EAD} is the mean area of an EAD. The magnitude of N_f is calculated via the expression: $N_f = N_A \times N_c \times V_M$, where N_A is Avogadro's constant [22]. The latter parameter is determined empirically; the major axis length of the 500 endosome sample was quantified through image based analysis, the mean, standard deviation and the lower and higher extremities were determined to be 213, 102, 62 and 497 nm respectively. There magnitudes are congruent with that measured through stochastic optical reconstruction microscopy [30]. We approximate the EAD capture area in our simulations to be circular given by $A_{EAD} = \pi R_E^2$.

Results

Figure 3(a) plots the PMFs corresponding to the experimentally determined number of NPs per agglomerate, x [11, 15]. The PMF of x measured at 0-h in media, $P^M(x)$, is the black curve with circle markers, the PMF corresponding to the number NPs per endosome measured after 1 h, $P^E(x)$, is the red curve with square markers. In both experimental cases, 500 randomly selected NP agglomerates/aggregates were selected and imaged via TEM, the number of distinct NPs within each cluster was determined via image analysis routines run on MATLAB [11].

To capture the observed variability associated with x, both curves in figure 3(a) are plotted on a semi-log x-axis. In media, x varies over the interval 1 to ~800 NPs; TEM images in figures 2(b) and (c), show examples from within the range, where the centroid positions of each individual NP within the agglomerate (red dots) is also shown [11]. Similarly, figures 2(d) and (e) display TEM images of low and high NP aggregate densities (17 and 320 NPs respectively) within endosome compartments, where x now spans the extended interval 1 to ~1500 NPs. Comparing $P^M(x)$ and $P^E(x)$, it is evident that the most probable magnitude of x has increased by two orders of magnitude (from 1 to 546 NPs), suggesting an accumulation of distinct NP agglomerates occurs during the endocytic process. Accumulation of NP agglomerates can take place at the cell surface within the lifetime of the EAD or may occur between early endosomes post internalization. In our methodology the exact biophysical mechanism(s) cannot be identified, but we have confidence that they have occurred due to the observed positive shift shown by the respective PMFs over the duration of the experiment.

The experimental data in figure 3 is recast to the equivalent cumulative distribution function (CDF) form in figure 4; classification of curve colours/markers is preserved, i.e. the CDFs in figure 4(a), $F^M(x)$ and $F^E(x)$, correspond to

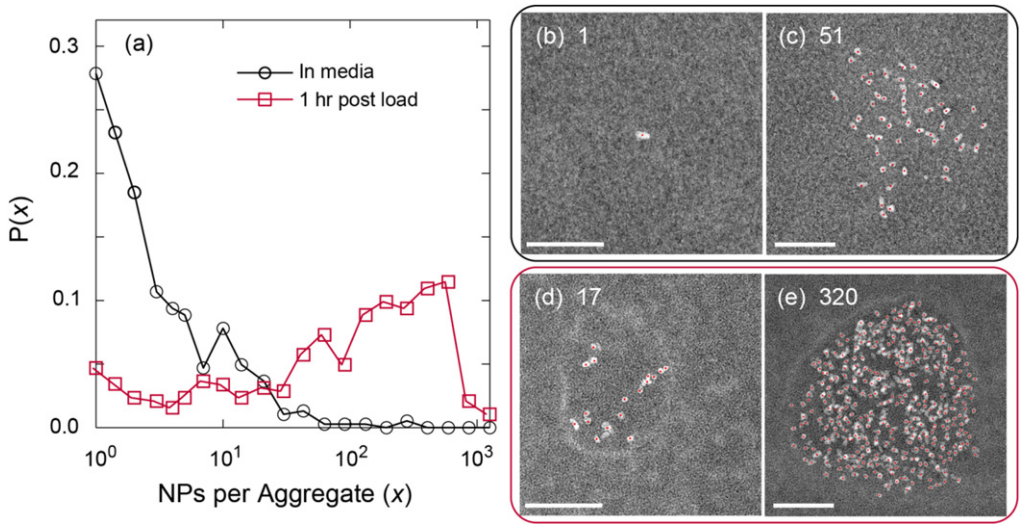

Figure 3. (a) PMFs of the number of constituent nanoparticles measured per cluster in media and within endosome compartments 1 h post nanoparticle load, black and red curves (circle/square markers) respectively. 500 clusters for each situation were examined to generate the PDFs. (b) and (c) TEM images of two typical NP clusters containing 1 and 51 individual NPs respectively; both images were measured in the media surrounding the cellular population. Figures (d) and (e) display TEM images of two endosomes containing NP clusters, the total NP load in the first is 17 NPs and 320 NPs in the second. Bright field TEM image contrast has been inverted such that NPs give white contrast and their identification by the image analysis script is shown as red dots. The scale bar for image (b) is 60 nm, for image (c) is 75 nm, for image (d) and (e) is 100 nm.

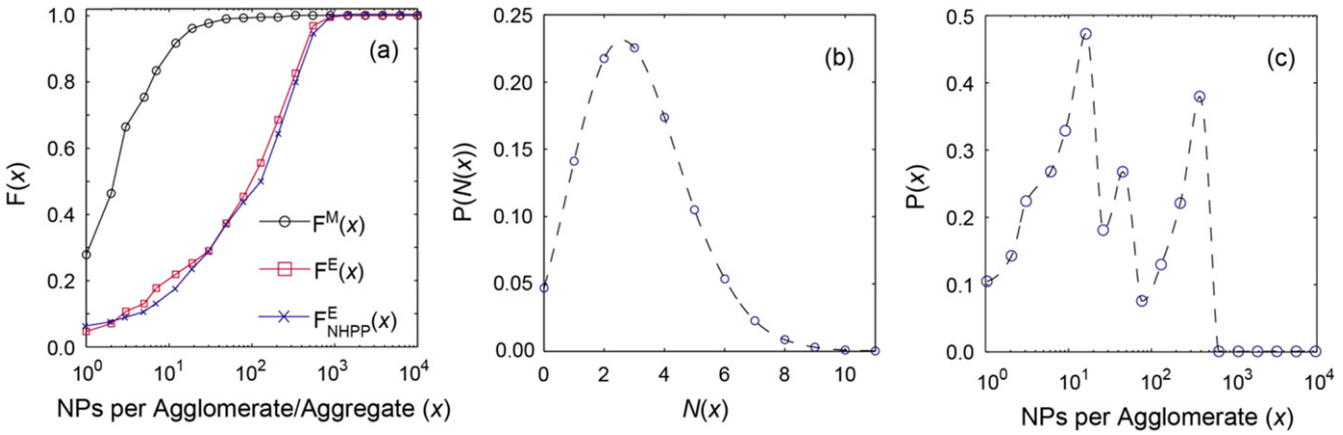

Figure 4. Comparison of the CDFs associated with the number of NPs per agglomerate measured experimentally and that predicted via the NHPP. (a) The black curve with circle markers and the red curve with square markers are the CDFs of the measured data at 0 h in media and 1 h post NP load within endosome compartments respectively (i.e. $F^M(x)$ and $F^E(x)$). The blue curve with 'x' markers is the optimized CDF predicted by the NHPP methodology, $F^E_{\mathrm{NHPP}}(x)$; the mean lifetime of the EAD was determined to be $\tau = 63$ s when $R_E = 213$ nm. A two-sample Kolmogorov–Smirnov test on $F^E(x)$ and $F^E_{\mathrm{NHPP}}(x)$ does not reject the null hypothesis at a significance level of 1% (p-value of 0.999). (b) The data points (circle markers) show the PMF associated with the predicted number NP agglomerates per EAD. The PMF is from 500 simulated EADs using the optimized value of τ and the sample average endosome radii. The data is fitted by the Poisson distribution (black dashed line) which predicts that a mean number of ~3 NP agglomerates in media combine to form larger aggregates measured within the endosome. (c) Here the data points (circle markers) indicate the PMF associated with the number of NPs per agglomerate that will merge across the endosome population.

that generated from experimental measurements of NP agglomerates in cell culture media and within endosome compartments respectively. In alignment with that measured experimentally, we evaluate equation (5) for 500 trials and estimate the number of NPs per endosome N_E for each trial. From this data we can calculate $F^E_{\mathrm{NHPP}}(x)$, an in silico predicted CDF via the NHPP. $F^E_{\mathrm{NHPP}}(x)$ is also displayed in figure 4(a) as the blue curve with 'x' markers. A statistical assessment of $F^E_{\mathrm{NHPP}}(x)$ and $F^E(x)$ through application of a two-sample Kolmogorov–Smirnov test does not reject the null hypothesis at a significance level of 1% (p-value of 0.999), suggesting that both distributions are equivalent. The accuracy of fit between $F^E_{\mathrm{NHPP}}(x)$ and $F^E(x)$ was iteratively achieved through optimization of the magnitude of the mean lifetime of an EAD, τ, the models only fitting parameter. Throughout the optimization process the mean EAD radii R_E was fixed at 213 nm (sample mean of the 500 TEM images), this magnitude is comparable to that of clathrin-coated pits

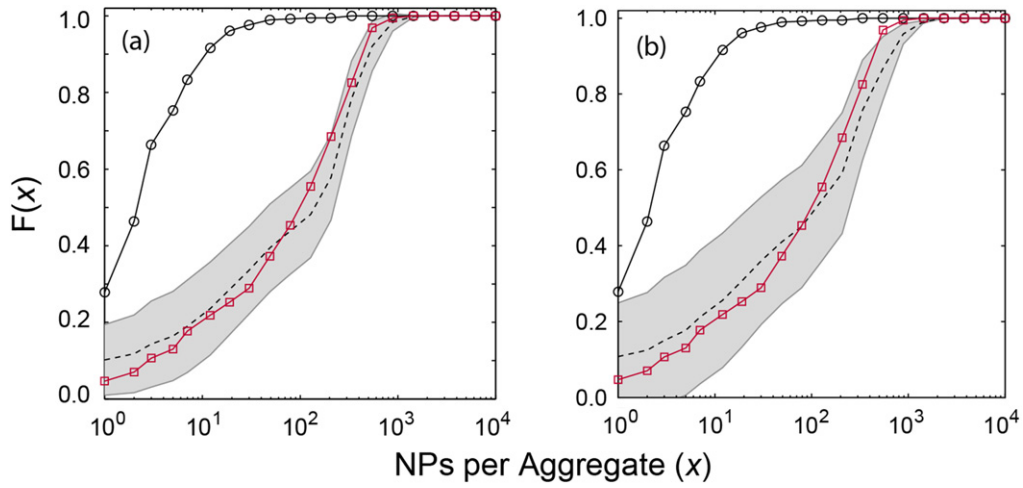

Figure 5. Sensitivity analysis of model (a) the magnitude of grey shaded area is ± one standard deviation of the mean value of $F^{E}_{\mathrm{NHPP}}(x)$ when we let R_E range over the interval [62, 497] nm whilst τ remains fixed at its optimum value (63 s). (b) The magnitude of grey shaded area is ± one standard deviation the mean value of $F^{E}_{\mathrm{NHPP}}(x)$ when R_E is fixed at the sample average (213 nm) and the magnitude of the lifetime associated with an EAD varies over the range [30, 240] seconds.

measured through stochastic optical reconstruction microscopy [30]. Location of the optimized lifetime value τ was established through numerical minimization of the L_2-norm of $F^{E}_{\mathrm{NHPP}}(x)$ and $F^{E}(x)$. Thus the optimized mean lifetime of an EAD was found to be 63 s, corresponding favourably to the lifetimes measured directly through high-resolution microscopy techniques [27, 28].

At the optimized value of τ and R_E fixed at 213 nm, we calculate the PMF associated with the number of constituent NP agglomerates per EAD, $N(x)$, over the 500 trials. The PMF of $N(x)$, $P(N(x))$, is displayed in figure 4(b) (circle markers) also shown by the black dashed line is a Poisson distribution fit to the calculated data (p-value—0.001). The mean rate ($\lambda(N(x)) = 3.05$) of the Poisson distribution indicates that ~3 distinct NP agglomerates merge within the lifetime of the EAD to form a larger internalized aggregate. Figure 4(c) is the PMF of the NP agglomerates that will undergo fusion in order to optimize best fit of the in-silico endosome population.

The main features of figure 4(c) indicate that the most probable NP agglomerates that undergo a fusion event are those containing 10–20 NPs, and those containing 300–400 NPs, additionally there is a low probability that agglomerates containing ~100 NPs will merge and zero probability of individual agglomerates >800 as they have not been detected experimentally, so are not sampled. These features approximately reflect the mean rate of transport of the NP agglomerates to the EADs generated by the ISDD model (see materials and methods—ISDD figure 2). The ISDD predicts high rates of transport to the cell surface for small (<10 NPs) and large (>300 NPs) agglomerates via diffusion and sedimentation respectively and a relatively slow transport of agglomerates that contain approximately 100 NPs. Thus, on average combinations of such NP agglomerates provides the mechanism that translates $P^{M}(x)$ to $P^{E}(x)$. The ISDD model also suggests relatively low numbers of 100 NP agglomerates in the internalized dose, however, even though there is a relative drop in probability at this size (see figure 3(a)) it is not expected to be significant as there is a strong likelihood that agglomerates of this magnitude can be created via the high probabilities associated with agglomerates of size 10–50 NPs combining.

Although the actual biological spatiotemporal location of the amalgamation events cannot be determined, the fact that we can statistically acknowledge their average occurrence and dispersion indicates specific properties of the cell-line/NP system. In particular, the PMF provides unresolved experimental information of how NP agglomerate dosage is transformed through endocytosis, one of the key factors limiting the development of nanomedicine based therapeutics and technologies.

To test the sensitivity of our methodology we investigated how the solution, i.e. $F^{E}_{\mathrm{NHPP}}(x)$, varied if we (i) fixed the mean lifetime of the EAD at its previously optimized value of 63 s and varied the magnitude of R_E contiguously from 62 to 497 nm (the extremities of the experimentally measured range) and (ii) holding R_E fixed at 213 nm and varying τ over the interval [30, 300] seconds. For every iteration, 500 trials of equation (5) (reflecting the 500 measured endosomes) and the corresponding CDF ($F^{E}_{\mathrm{NHPP}}(x)$) is deduced. After each in-silico experiment the mean and standard deviations of the respective CDF series is calculated, additionally the mean number of fusion events that have occurred for all iterations of the CDFs series is calculated and found to be ~3 in both cases. The means (dashed black lines) and standard deviations (grey areas) associated with the variation of R_E and τ are displayed in figures 5(a) and (b) respectively. For reference both $F^{M}(x)$ and $F^{E}(x)$ are also indicated on both figures, black line circles markers and red line square markers respectively.

The variation of R_E corresponds physically to variation of the capture area associated with EADs; reduction of R_E

vastly increases the variability of predicted $F(x)$ especially for aggregates having $x < 100$ corresponding to the diffusion dominated transport regime. For $x > 100$, $F(x)$ does not deviate substantially from the optimum CDF shown in figure 4(a) suggesting that at least one of the three fusion events likely to occur is between relatively large agglomerates. As the magnitude of R_E increases in size past the sample mean the calculated CDFs are shifted positively in x. This is unsurprising as (i) equation (6) indicates that the number of agglomerates at the EAD will increase proportionally to the magnitude of R_E, and (ii) a large proportion of these agglomerates will be that driven by sedimentation as this on average is the dominant transport mechanism an is associated with the larger NP agglomerates. Figure 5(b) illustrates the variability of $F(x)$ when the lifetime of the EAD is varied from half its optimized value to that five times greater than its optimized value and the capture area of the EAD is fixed at ~0.014 μm^2. The general features of the variability follow that observed for R_E variation, i.e. larger fluctuation in $F(x)$ for $x < 100$ for small EAD lifetimes, and a positive shift in magnitude of $F(x)$ as the lifetime is increased well beyond the optimized value of 63 s. In an analogous manner to that previously described, this shift is not surprising as we are again increasing the possibility of larger agglomerate fusion events as they have the dominant transport mechanism in these simulations.

The generally low dispersion observed for $F(x)$ (for $x > 100$ NPs) is interesting and suggests that the net NP aggregation by endosomes is insensitive to both the magnitude of the EAD and its mean lifetime. The former feature reflects TEM measurements that indicate small NP agglomerates are found within much larger endosome compartments and equally many large NP agglomerates are found within similar sized compartments (e.g. figures 3(d) and (e)). Ongoing and future experiments will quantify this feature further. The larger fluctuations of $F(x)$ for small x, in both cases, is related to increased sampling variability and will have a major impact on the predictability of dosage when no agglomeration is present, i.e. for monodispersions of NPs.

Discussion

This study directly addresses key factors limiting the development of nanomedicine based therapeutics; we precisely quantify actual NP dosage as opposed to that perceived, in doing so we encapsulate the innate heterogeneity of the nanotheraputic state. We provide a robust methodology that allows the trafficking of NP dosage across biological barriers to be understood quantitatively which provides the basis for predictive modelling of nanopharmacology. In this study, we have focused on quantifying biological barrier trafficking of Qtracker 705 quantum dots exposed to U-2 OS cells in McCoy's 5a medium media.

The methodology couples high spatial resolution TEM with pertinent physical models that together are statistically sampled to infer the dynamical properties of a NP dose. Specifically, through TEM measurements [11] we characterize the aggregating properties associated with NP agglomerates at two distinct spatiotemporal biological positions (i) in biological media and (ii) within cellular endosome compartments in human osteosarcoma cells [15, 17, 19–21, 23, 24]. The statistical profile of NP dose at these distinct spatiotemporal positions was captured by PMFs that summarize the properties of 500 quantum dot NP agglomerates, which describe the heterogeneity of particle number within measured agglomerates. We detailed and developed a stochastic transfer function (STF) that permits evolution of states from $P^M(x)$ to $P^E(x)$. The STF has two principal components, firstly the previously reported ISDD model [26] is embedded to provide a mean rate of NP agglomerate transport to the cell surface and (ii) system heterogeneity simulated through application of a nonhomogeneous Poisson distribution, which stochastically determines agglomerate arrival at the cell surface where it may be part of and endocytic event and subsequently internalized by a cell. The STF's principal fitting parameter reflects the lifetime of an endocytic event, its optimized magnitude was found to be commensurate with direct measurements of clathrin-coated pits through high-resolution microscopy techniques [27, 28]. Further analysis of the STF provides previously unresolved dynamics of the NP agglomerate traverse across the cell membrane, quantifying statistically agglomerates fusion as NP dose is translated from cell-culture media to endosome vesicles. Through optimization and sampling of the statistical methodology we are confident in stating that the heterogeneity of the internalized NP dose (reported previously [15, 24]) is a result of the initial, inhomogeneous dispersion of the NPs in the cell culture media used for particle exposure.

This manuscript has developed a statistical framework for the detection (by TEM), quantification and prediction of quantum dots dispersed in media and following uptake by any cells all at the scale of the individual quantum dot. *Future work* will examine and assess how specific variables of the system, e.g. cell/NP type, NP surface coating, concentration or applied exposure dose of NPs have on the heterogeneity measured at both temporal locations and how these are statistically translated across the biological membrane. Additionally, we will combine the methods presented here with that previously developed [15] to fundamentally link high-throughput flow cytometry measurements with TEM based statistics to provide accurate assessment of actual NP dosage and its evolution and redistribution across a large cellular population over significant periods.

Acknowledgments

This work was supported by the Engineering and Physical Sciences Research Council, U.K. under Grants EP/H008683/1 and EP/M000621/1 Swansea and EP/H008578/1 Leeds.The authors would like to thank A Warley, K Brady, and F Winning (Centre for Ultrastructural Imaging, King's College, London, U.K.) for pelleting and sectioning the cells for TEM analysis.

References

[1] Brannon-Peppas L and Blanchette J O 2004 Nanoparticle and targeted systems for cancer therapy *Adv. Drug Deliv. Rev.* **56** 1649–59

[2] Kawasaki E S and Player A 2005 Nanotechnology, nanomedicine, and the development of new, effective therapies for cancer *Nanomedicine* **1** 109

[3] Zhang L, Gu F X, Chan J M, Wang A Z, Langer R S and Farokhzad O C 2007 Nanoparticles in medicine: therapeutic applications and developments *Clin. Pharm. Theraputics* **83** 769

[4] Na H B, Song I C and Hyeon T 2009 Inorganic nanoparticles for MRI contrast agents *Adv. Mater.* **21** 2133–48

[5] Montes-Burgos I, Walczyk D, Hole P, Smith J, Lynch I and Dawson K 2010 Characterisation of nanoparticle size and state prior to nanotoxicological studies *J. Nanoparticle Res.* **12** 47–53

[6] Warheit D B 2008 How meaningful are the results of nanotoxicity studies in the absence of adequate material characterization? *Toxicological Sci.* **101** 183–5

[7] Elsaesser A, Taylor A, Staats de Yanés G, McKerr G, Kim E-M, O'Hare E and Howard C V 2010 Quantification of nanoparticle uptake by cells using microscopical and analytical techniques *Nanomedicine* **5** 1447–57

[8] Albanese A and Chan W C W 2011 Effect of gold nanoparticle aggregation on cell uptake and toxicity *ACS Nano* **5** 5478–89

[9] Singh N, Jenkins G J S, Nelson B C, Marquis B J, Maffeis T G G, Brown A P, Williams P M, Wright C J and Doak S H 2012 The role of iron redox state in the genotoxicity of ultrafine superparamagnetic iron oxide nanoparticles *Biomaterials* **33** 163–70

[10] Gosens I, Post J A, de la Fonteyne L J J, Jansen E H J M, Gues J W, Cassee F R and de Jong W H 2010 Impact of agglomeration state of nano- and submicron sized gold particles on pulmonary inflammation *Part. Fibre Toxicology* **7** 37

[11] Hondow N, Brydson R, Wang P, Holton M D, Brown M R, Rees P, Summers H D and Brown A 2012 Quantitative characterization of nanoparticle agglomeration within biological media *J. Nanoparticle Res.* **14** 977

[12] Xiao Y, Forry S P, Gao X, Holbrook R D, Telford W G and Tona A 2010 Dynamics and mechanisms of quantum dot nanoparticle cellular uptake *J. Nanobiotechnol.* **8** 13

[13] Krpetic Ž, Saleemi S, Prior I A, Sée V, Qureshi R and Brust M 2011 Negotiation of intracellular membrane barriers by TAT-modified gold nanoparticles *ACS Nano* **5** 5195–201

[14] Shapero K, Fenaroli F, Lynch I, Cottell D C, Salvati A and Dawson K A 2011 Time and space resolved uptake study of silica nanoparticles by human cells *Mol. BioSyst.* **7** 371–8

[15] Summers H D, Brown M R, Holton M D, Tonkin J A, Hondow N, Brown A P, Brydson R and Rees P 2013 Quantification of nanoparticle dose and vesicular inheritance in proliferating cells *ACS Nano* **7** 6129–37

[16] Rosman C, Pierrat S, Henkel A, Tarantola M, Schneider D, Sunnick E, Janshoff A, Sönnichsen C and New A 2012 Approach to assess gold nanoparticle uptake by mammalian cells: combining optical dark-field and transmission electron microscopy *Small* **8** 3683–90

[17] Errington R J, Brown M R, Silvestre O F, Njoh K L, Chappell S C, Khan I A, Rees P, Wilks S P, Smith P J and Summers H D 2010 Single cell nanoparticle tracking to model cell cycle dynamics and compartmental inheritance *Cell Cycle* **9** 121–30

[18] Manshian B B, Soenen S J, Al-Ali A, Brown A, Hondow N, Wills J, Jenkins G J S and Doak S H 2015 Cell type dependent changes in CdSe/ZnS quantum dot uptake and toxic endpoints *Toxicological Sci.* at press doi:10.1093/toxsci/kfv002

[19] Brown M R, Rees P, Wilks S, Summers H D, Errington R J, Njoh K L, Chappell S C, Smith P J and Leary J F 2007 Computational simulation of optical tracking of cell populations using quantum dot fluorophores ed M G S Calder *Proc. Computational Methods in Systems Biology* pp 96–105

[20] Brown M R, Summers H D, Rees P, Chappell S C, Silvestre O F, Khan I A, Smith P J and Errington R J 2010 Long-term time series analysis of quantum dot encoded cells by deconvolution of the autofluorescence signal *Cytometry* A **77A** 925–32

[21] Brown M R, Summers H D, Rees P, Smith P J, Chappell S C and Errington R J 2010 Flow-based cytometric analysis of cell cycle via simulated cell populations *PLoS Comput. Biol.* **6** e1000741

[22] Summers H 2013 Frontiers of nanoscience *Nanomedicine* ed H Summers pp 26

[23] Summers H D, Errington R J, Smith P J, Chappell S, Rees P, Brown M R and Leary J F 2008 Cell-population tracking using quantum dots in flow cytometry *Proc. Soc. Photo-Opt. Insrum. Eng.* **6865** L8650–8650

[24] Summers H D, Rees P, Holton M D, Brown M R, Chappell S C, Smith P J and Errington R J 2011 Statistical analysis of nanoparticle dosing in a dynamic cellular system *Nat. Nanotechnology* **6** 170–4

[25] Nakase I *et al* 2004 Cellular uptake of arginine-rich peptides: roles for macropinocytosis and actin rearrangement *Mol. Ther.* **10** 1011–22

[26] Hinderliter P M, Minard K R, Orr G, Chrisler W B, Thrall B D, Pounds J G and Teeguarden J G 2010 ISDD: A computational model of particle sedimentation, diffusion and target cell dosimetry for *in vitro* toxicity studies *Part. Fibre Toxicology* **7** 36

[27] Ehrlich M, Boll W, Van Oijen A, Hariharan R, Chandran K, Nibert M L and Kirchhausen T 2004 Endocytosis by random initiation and stabilization of clathrin-coated pits *Cell* **118** 591–605

[28] Hansen S H, Sandvig K and Van Deurs B 1992 Internalization efficiency of the transferrin receptor *Exp. Cell Res.* **199** 28

[29] Alberts B, Bray D, Hopkin K, Johnson A, Lewis J, Raff M, Roberts K and Walter P 2009 *Essential Cell Biology* (New York: Garland Science)

[30] Huang B, Wang W, Bates M and Zhuang X 2008 Three-dimensional super-resolution imaging by stochastic optical reconstruction microscopy *Science* **319** 810–3

[31] Falconer K J 2003 *Fractal Geometry: Mathematical Foundations and Applications* 2nd edn (Chichester: Wiley)